Temporal interference stimulation targets deep brain regions by modulating neural oscillations

Zeinab Esmaeilpour[a,*], **Greg Kronberg**[a], **Davide Reato**[b], **Lucas C. Parra**[a], **Marom Bikson**[a]

[a]Department of Biomedical Engineering, The City College of the City University of New York, New York, NY, USA

[b]Champalimaud Centre for the Unknown, Neuroscience Program, Lisbon, Portugal

Abstract

Background: Temporal interference (TI) stimulation of the brain generates amplitude-modulated electric fields oscillating in the kHz range with the goal of non-invasive targeted deep brain stimulation. Yet, the current intensities required in human (sensitivity) to modulate deep brain activity and if superficial brain region are spared (selectivity) at these intensities remains unclear.

Objective: We developed an experimentally constrained theory for TI sensitivity to kHz electric field given the attenuation by membrane low-pass filtering property, and for TI selectivity to deep structures given the distribution of modulated and unmodulated electric fields in brain.

Methods: The electric field threshold to modulate carbachol-induced gamma oscillations in rat hippocampal slices was determined for unmodulated 0.05–2 kHz sine waveforms, and 5 Hz amplitude-modulated waveforms with 0.1–2 kHz carrier frequencies. The neuronal effects are replicated with a computational network model to explore the underlying mechanisms, and then coupled to a validated current-flow model of the human head.

Results: Amplitude-modulated electric fields are stronger in deep brain regions, while unmodulated electric fields are maximal at the cortical regions. Both experiment and model confirmed the hypothesis that spatial selectivity of temporal interference stimulation depends on the phasic modulation of neural oscillations only in deep brain regions. Adaptation mechanism (e.g. $GABA_b$) enhanced sensitivity to amplitude modulated waveform in contrast to unmodulated kHz and produced selectivity in modulating gamma oscillation (i.e. Higher gamma modulation in amplitude modulated vs unmodulated kHz stimulation). Selection of carrier frequency strongly affected sensitivity to amplitude modulation stimulation. Amplitude modulated stimulation with 100 Hz carrier frequency required ~5 V/m (corresponding to ~13 mA at the scalp surface), whereas, 1 kHz carrier frequency ~60 V/m (~160 mA) and 2 kHz carrier frequency ~80 V/m (~220 mA) to significantly modulate gamma oscillation. Sensitivity is increased (scalp current required decreased) for theoretical neuronal membranes with faster time constants.

*Corresponding author: znb.esmailpoor@gmail.com (Z. Esmaeilpour).

Conclusion: The TI sensitivity (current required at the scalp) depends on the neuronal membrane time-constant (e.g. axons) approaching the kHz carrier frequency. TI selectivity is governed by network adaption (e.g. $GABA_b$) that is faster than the amplitude-modulation frequency. Thus, we show neuronal and network oscillations time-constants determine the scalp current required and the selectivity achievable with TI in humans.

Keywords

Temporal interference; Interferential stimulation; Amplitude modulation; Gamma oscillation; Non-invasive deep brain stimulation

1.   Introduction

Temporal Interference (TI) stimulation delivers high frequency (kHz) sinusoidal stimulation to multiple electrodes on the scalp, where small differences in frequency (e.g. 2 and 2.10 kHz) between electrodes results in an Amplitude-Modulated (AM) electric field deep in the brain (e.g. 2.05 kHz "carrier" whose amplitude is modulated with a "beat" of 100 Hz) [1]. While targeted deep brain structures are exposed to an amplitude-modulated kHz electric fields, superficial cortex is stimulated with higher magnitude unmodulated kHz electric fields. The effectiveness of temporal interference stimulation [2] thus depends on: 1) steerability of the amplitude-modulated electric fields to targeted deep brain regions [3,4]; 2) the extent to which neuronal activity is more responsive to amplitude-modulated high-frequency electric fields compared to unmodulated electric field (selectivity); 3) the current intensity requirement at the scalp level to produce sufficiently strong amplitude-modulated kHz fields deep in the brain (sensitivity).

The effects of electrical stimulation on neuronal oscillations are often analyzed because of their sensitivity to external electric fields [5–7] and involvement in a broad range of cognitive functions and diseases [8–10]. Conventional transcranial Alternating Current Stimulation (tACS) applies ~2 mA at the scalp level, producing electric fields up to ~0.8 V/m in the human brain [11]. In animal models, such small sinusoidal electric fields can modulate oscillations at stimulation frequencies below 100 Hz [6,12–15] but not evidently for weak kHz frequency stimulation [15,16]. Generally, there is a severe trade-off between the use of kHz stimulation frequencies and amplitudes required for brain stimulation [17–19]. Estimates of the temporal interference electric fields required for acute neuronal modulation in mouse range from 60 to 350 V/m [1,4] corresponding to 167–970 mA at the human scalp [20]. Applying kHz tACS with currents of only 1 mA produces mixed effects in human experiments [21], with loss of efficacy when the waveform is not continuous [22]. The foundation of temporal interference stimulation is the report that neural firing is more sensitive to amplitude-modulated than unmodulated kHz stimulation [1]. However, the low-pass properties of neuronal membranes [15,23] would a priori predict equal attenuation of both unmodulated kHz and amplitude-modulated kHz stimulation [2,18] – making amplitude-modulated kHz stimulation as ineffective as unmodulated kHz stimulation. Here, we integrate and reconcile these confounding findings.

Our goal was to develop an experimentally constrained theory for what makes the CNS sensitive to amplitude-modulated high-frequency (kHz) stimulation, how this sensitivity differs compared to unmodulated sinusoidal stimulation at low and high frequencies, and link the sensitivity and selectivity to the spatiotemporal electric fields produced across the brain during temporal interference stimulation. The hippocampal brain slice model is among the most characterized systems in neuroscience and exhaustively tested in screening the effects of electrical stimulation [6,15,24–26]. Specifically, gamma oscillations have been previously shown to be most sensitive to conventional forms of electrical stimulation, with effects reliably predicted by a computational network model [6]. Here, we used this system to test the effects of amplitude-modulated kHz stimulation and contrast outcomes to unmodulated kHz and low-frequency sinusoidal stimulation. We coupled this data into a multi-scale model of temporal interference brain current flow and network neuromodulation. We showed that temporal interference stimulation depends on the value of phasic modulation of neural oscillations in deep brain regions, as opposed to steady increases driven by unmodulated kHz fields at the cortex. Sensitivity depends on a time constant of membrane polarization close to carrier frequency, while selectivity depends on network homeostatic kinetics that are faster than the frequency (beat) of amplitude modulation.

2. Materials and methods

2.1. Hippocampal slice preparation

All animal experiments were carried out in accordance with guidelines and protocols approved by the Institutional Animal Care and Use Committee at The City College of New York, CUNY. Hippocampal brain slices were prepared from male Wistar rats aged 3–5 weeks old, which were deeply anaesthetized with ketamine (7.4 mg kg−1) and xylazine (0.7 mg kg−1) and sacrificed by cervical dislocation. The brain was quickly removed and immersed in chilled (2–6 °C) dissecting solution containing (in mM) 110 choline chloride, 3.2 KCl, 1.25 NaH2PO4, 26 NaHCO3, 0.5 CaCl2, 7 MgCl2, 2 sodium ascorbate, 3 sodium pyruvate, 10 D-glucose. Transverse hippocampal slices (400 μm thick) were cut using a vibrating microtome (Campden Instruments, Leicester, England) and transferred to a recovery chamber for 30 min at 34 °C with a modified artificial cerebrospinal fluid (ACSF) containing (in mM) 124 NaCl, 3.2 KCl, 1.25 NaH2PO4, 26 NaHCO3, 2.5 CaCl2, 1.3 MgCl2, 2 sodium ascorbate, 3 sodium pyruvate, and 25 D-glucose. Slices were then transferred to a holding chamber for at least 30 min (or until needed) at 30 °C with ACSF containing (in mM) 124 NaCl, 3.2 KCl, 1.25 NaH2PO4, 26 NaHCO3, 2.5 CaCl2, 1.3 MgCl2, and 25 D-glucose. After 60 min, slices were then transferred to a fluid–gas interface recording chamber (Hass top model, Harvard Apparatus, Holliston MA, USA) at 34 °C. All solutions were saturated with a gas mixture of 95% O2–5% CO2. All reagents were purchased from Sigma Aldrich (St. Louis MO, USA). Gamma oscillations were induced by perfusing the slices with ACSF containing 20 μM carbachol (carbamoylcholine chloride). The frequency of gamma oscillations induced by carbachol is a function of its concentration in the superfusate [27]. The carbachol concentration used in this study (i.e. 20 μM) generated gamma at a frequency between 20 and 40 Hz, in agreement with previous results [6,27].

2.2. Extracellular recordings

Recordings of extracellular field potentials in the pyramidal layer of CA3a region of hippocampus were obtained using glass micropipettes (15 MΩ pulled on a P-97, Sutter instruments) filled with ACSF. Data acquisition and electrical stimulation were controlled by Power1401-625 kHz hardware and Signal software Version 6.0 (Cambridge Electronic Design (CED), Cambridge, UK). Voltage signals were amplified (1×), analog low pass filtered (20 kHz; Model 3000 differential amplifier, A-M systems, Carlsberg WA, USA) and digitized (20 kHz, Power1401-625 kHz and Signal, CED, Cambridge, UK). To reduce noise and stimulation artifacts, the voltage recordings were always performed relative to an iso-potential electrode placed in bath (Fig. 1, B1). Electrophysiology experiments with kHz electric field stimulation must carefully account for the fidelity of delivered stimulation and recording artifacts [28]. Field recordings overcome potential limitations of intracellular recording under kHz field such as current collection by the capacitive-walled microelectrode leading to artifactual intracellular stimulation [29] or possible amplifier distortion [30].

2.3. Electrical field stimulation

The generation of amplitude-modulated or unmodulated kHz fields in distinct brain regions is the fundamental rationale for temporal interference stimulation [1,2,31] and approaches to optimize it [3,4,19,32]. Under the quasi-uniform assumption [33–35], the electric field amplitude and waveform generated in a brain ROI can be applied across an in vitro system. Spatially uniform electric fields were applied to slices with varying frequencies and intensities by passing current between two parallel Ag–AgCl wires (1 mm diameter, 12 mm length, 10 mm apart) placed in the recording chamber on opposite sides of the brain slice [6,23]. Field waveforms were generated by function generator (Arbitrary function generator, AFG1062, 60 MHz, 300 Ms/s, Tektronix, USA) and converted to a controlled current source stimulus by a custom high band-width voltage-controlled isolated current source [29]. Unless otherwise stated, the electric field reported throughout the manuscript is the peak electric field for each waveform. Slices were oriented so that the resulting electric field was parallel to the main somato-dendritic axis of CA3a pyramidal neurons (perpendicular to pyramidal cell layer) (Fig. 1B1). Stimulation was applied 30–45 min after application of carbachol when the intensity and frequency of gamma oscillations were stabilized. Before each recording, the applied current intensity was calibrated by measuring the electric field (voltage difference between two recording electrodes separated by 0.4 mm in the slice) [36,37]. In a piloting phase (not shown), different sensitivities were evident across waveforms, such that waveform specific electric field ranges showed dose dependency with comparable efficacy.

2.4. Power analysis and statistics

Signals were recorded in frames of 7 s (1.5 s before and 3.5 s after stimulation) and stimulation was applied for 2 s. Stimulation artifacts were minimized by subtracting the voltage in an iso-potential reference electrode from the recording electrode in the slice (Fig. 1). Spectrograms were computed (200 m s hamming window, 90% overlap) on individual 7 s frames and averaged over 100 frames for each stimulation condition (i.e. frequency, waveform and amplitude). Normalized power was measured as a power ratio normalized

by pre-stimulation power in the frequency band of the endogenous oscillation. In case of 100 Hz stimulation (i.e. sine 100 Hz and 5 Hz-AM-100 Hz), which caused ~5 Hz shift in endogenous gamma oscillation during stimulation, gamma power was measured and quantified in the center frequency of the oscillation specific to each interval (i.e. baseline, stimulation).

To quantify the mean effect of stimulation we defined the static modulation as the mean power in the gamma band (20–40 Hz) during the final 1 s of stimulation in each frame divided by the mean gamma power immediately preceding stimulation (1 s). To capture the dependence of gamma modulation on the phase of the stimulation waveform, we defined a dynamic modulation metric. For 5 Hz sine stimulation, dynamic modulation was the power ratio of positive field over negative fields. For AM-high-frequency stimulation, dynamic modulation was the ratio of the gamma power during the peak interval to gamma power during the trough interval. Unless otherwise stated, results are reported as mean ± SEM; n = number of slices.

All the statistical analysis were done in R (R core Team, 2018) [38]. lme4 [39] was used to perform a linear mixed effect analysis between different stimulation intensities. Stimulation intensity was used as fixed effect for each tested waveform. Significance ($p < 0.05$) was characterized by Type III analysis of variance (ANOVA) followed by post hoc test with Tukey test for multiple comparisons. Unless otherwise stated, statistical significance refers to $p < 0.05$.

2.5. Computational head model

We adapted an existing detailed head model with 1 mm resolution to predict the spatial distribution of electric fields across the human brain during temporal interferential stimulation. Briefly, the model was segmented into tissues with different conductivities (scalp, fat, skull, CSF, air, grey and with matter). The model was meshed using ScanIP and solved using a finite element modeling software (COMSOL). We used two independent pairs of electrodes: FT7 and P7 on the left side and FT8 and P8 on the right hemisphere. The spatial distribution of amplitude-modulated electric field was measured in the posterior/anterior direction (see [3] for technical details). We assumed a quasi-static approximation to Maxwell's equation in the simulation. This approximation is suitable for frequencies used in this study (i.e. 1, 2 kHz) as displacement current can be neglected [1,40,41].

2.6. Network model

A network of excitatory and inhibitory neurons was used to explain our results in hippocampal brain slices. The local recurrent CA3 circuit was simulated using a model consisting of 800 excitatory and 250 inhibitory neurons (200 form synapses with $GABA_a$ dynamic, 50 from synapses with $GABA_b$). Each cell was modeled as a single-compartment, adaptive exponential integrate-and-fire neuron (AdEx) since it can produce a large variety of neuronal behaviors by changing few parameters [42]. The following differential equations describe the evolution of the membrane potential V(t) of each neuron:

$$C\frac{dV}{dt} = -g_L(V - E_L) + \Delta_T \exp\left(\frac{V - V_T}{\Delta_T}\right) + I_{syn} + I_N + I_{stim} - I_w \qquad (1)$$

$$\tau_w\frac{dI_w}{dt} = a(V - E_L) - I_w \qquad (2)$$

When the current drives the potential beyond V_T, the exponential term actuates a positive feedback which leads to upswings of the action potential. The upswing is stopped at a reset threshold which we fixed at $V_{thre} = -50\ mV$. When membrane voltage exceeded the reset threshold, the state variables were modified in the following manner:

$$if\ V > V_{thre}\ then \begin{cases} V \to V_{reset} \\ I_w \to I_w = I_w + b \end{cases} \qquad (3)$$

Parameters for both inhibitory and excitatory neurons are as follows: *Excitatory neurons* : $C = 100\ pF$, $E_L = -55\ mV$, $a = 2$, $b = 8$, $\tau_w = 400$, $T = 2.7$, $g_L = 100\ nS$, $V_T = -52\ mV$, $V_{reset} = -55\ mV$; *Inhibitory neurons* : $C = 100\ pF$, $E_L(GABA_a) = -62\ mV$, $E_L(GABA_b) = -67\ mV$, $a = 0$, $b = 0$, $\tau_w = 400$, $T = 1$, $V_T = -55\ mV$, $V_{reset}(GABA_a) = -62\ mV$, $V_{reset}(GABA_b) = -67\ mV$. The parameters used here for excitatory neurons correspond to regular spiking neurons whereas parameters for inhibitory neurons correspond to fast-spiking perisomatic-targeting neurons.

The network was structured such that neurons were connected randomly with uniform probability p_{ij} of connection between a postsynaptic neuron i and a presynaptic j, which depended on the type of pre and post-synaptic neuron: $p_{EE} = 0.15$, $p_{I_{GABA\,a},\,E} = 0.4$, $p_{I_{GABA\,b},\,E} = 1$, $p_{E,\,I_{GABA\,a}} = 0.4$, $p_{E,\,I_{GABA\,b}} = 0.4$, $p_{I_{GABA\,a},\,I_{GABA\,a}} = 0.4$, $p_{I_{GABA\,b},\,I_{GABA\,a}} = 0$, where E represents excitatory and I_{GABA_a}, I_{GABA_b} represent two different type of inhibitory neurons. The connectivity was sparser between excitatory neurons than other pairs [43,44]. The synaptic current $I_{syn,i}$ received by neuron i was the result of spiking activity of all connected pre-synaptic neurons j which can be decomposed into excitatory and inhibitory components: $I_{syn,\,i} = (E_e - V)g_i^{exc} + (E_i - V)g_i^{inh}$. Synaptic conductance g was modeled using a decaying exponential function. At each synaptic event, conductance was increased by factor W_{ij} and then it followed an exponential decrease with time constant T:

$$g = \begin{cases} \exp\left(-\frac{t - t^f}{\tau}\right) & t \geq t^f \\ 0 & t < t^f \end{cases} \qquad (4)$$

The total inhibitory and excitatory conductance that neuron i receives was calculated as follows:

$$g_i^{exc}(t) = \sum_j \sum_f^{exc} W_{ij} * g_{ij}\left(t - t_j^f\right) \tag{5}$$

$$g_i^{inh}(t) = \sum_j \sum_f^{inh} W_{ij} * g_{ij}\left(t - t_j^f\right) \tag{6}$$

where $\tau_{exc} = 5\ ms$, $\tau_{inh\ GABAa} = 8\ ms$[45] and $GABA_b$ conductance has 50 m s of delay and a longer time constant ($\tau_{inhGABAb} = 50\ ms$) [46]. The synaptic strengths were chosen to be uniformly distributed for $w_{E,E} \in [0, 0.3]$, $w_{I_{GABAa}, E} \in [0, 2]$, $w_{E, I_{GABAa}} \in [0.5, 2.5]$, $w_{I_{GABAa}I_{GABAa}} \in [0, 0.5]$, $w_{E, I_{GABAb}} \in [0, 0.5]$, $w_{I_{GABAb}, E} = 0.5$. In the absence of synaptic input from the network, each excitatory cell was subjected to Gaussian noise (SD = 0.5 nA) to simulate spontaneous activity of pyramidal cells under carbachol perfusion (I_N). The local field potential (LFP) reflects the activity of large number of neurons reflecting excitatory and inhibitory synaptic activity recorded in aggregate extracellularly. LFP signal was calculated by averaging all excitatory and inhibitory postsynaptic currents from the network (Fig. 1C2) [6].

Model of electric field in the network: The effect of stimulation was implemented as a small current (I_{stim}) injected into excitatory neurons [6,18,19,47]. This approach captures the induced membrane polarization in single compartments due to external electric field application and is experimentally verified [6,48,49]. The soma of inhibitory neurons were not polarized by the field, assuming a symmetric dendritic morphology [50]. This parsimonious model excludes a litany of additional cell types and compartment specific computations (see Discussion). It has been shown that 1 V/m produces ~0.2 mV polarization at low frequency (<7 Hz) [15]. In the present model, DC current intensity required to generate 0.2 mV membrane polarization was assumed to be equivalent to 1 V/m electric field ($I_{0.2\ mV\ polarization\ in\ DC} = 1\ V/m$). The waveform of AM high-frequency stimulation was constructed by subtracting two sinusoidal waveforms where f_c is the carrier frequency and f_m is the modulating frequency ($f_m = 5\ Hz$, $f_c = 0.1, 1, 2\ kHz$).

$$I_{stim} = \frac{I}{2}(\sin(2\pi(f_c + f_m)t) - \sin(2\pi f_c t)) \tag{7}$$

Generalized model: For all the conditions in the generalized model, network structure (connectivity and synaptic weights) followed the same probability distributions as described above in the network model that represented in vitro experiments. In order to evaluate the effect of membrane time constants on network sensitivity to temporal interference stimulation, membrane capacitance (C) was changed only for directly polarized excitatory cells. Membrane capacitance was modeled using $C = 40\ pF$ (lowest membrane time constant) and $C = 300\ pF$ (highest membrane time constant). For studying selectivity, in some simulations $GABA_b$ inhibition was removed by setting the weight of all $GABA_b$

synapses to zero ($W_{E, I_{GABAb}} = 0$). When varying parameters in the model, the noise current simulating the effect of carbochol in pyramidal cells (I_N) was adjusted to keep firing the rates of excitatory and inhibitory cells and the network oscillation frequency within the range of reported experimental data [51,52]. For visualization of the results in human head, false color maps were thresholded based on hippocampal experimental results (Fig. 3).

3. Results

3.1. Temporal interference current flow model

We begin with a computational model of the spatial distribution of electric field across the human brain, using a previously verified modeling pipeline [11,53]. We considered a standard temporal interference montage with two bipolar pairs of electrodes on opposite hemispheres (Fig. 1, A1) applying 1 kHz and 1.005 kHz sinusoidal stimulation with an exemplary amplitude of 167 mA. In regions where electric currents from each electrode pair intersects, the resulting electric field has a carrier frequency of 1.0025 kHz with an amplitude modulation (change in peak electric field) at 5 Hz. At the superficial cortex located near each electrode pair, electric field magnitudes reach peak values of ~80 V/m (Fig. 1A2). At these locations, the electric field was modulated minimally (amplitude-modulation of ~15%). In contrast, in deep brain regions amplitude-modulation of electric fields could be as high as 50% or more (Fig. 1A3), corresponding to changes of ~60 V/m at the 5 Hz beat frequency.

Both the electric field magnitude and amplitude-modulation scale linearly with the applied current. In cortex, unmodulated electric field magnitudes can reach ~0.48 V/m per mA applied current, while in deep brain areas amplitude-modulation of electric fields can reach ~0.36 V/m per mA applied current. Therefore, while amplitude-modulated kHz stimulation can be directed to deep brain regions, on the cortex electric field magnitudes will also be high, consistent with prior models [3,4].

3.2. Amplitude-modulated and unmodulated kHz stimulation of hippocampal brain slice oscillations

Adapting previous methods [23], uniform amplitude-modulated kHz, unmodulated kHz, and low-frequency AC fields were generated across hippocampal slices exhibiting gamma network oscillations (Fig. 1B1). Consistent with prior reports [6,52], 20 μM carbochol induced oscillatory activity in local field potentials measured in the CA3a region of the hippocampus (Fig. 1B2, B3). Oscillations were typically stable for over 3 h. Hippocampal gamma oscillation was chosen due to long standing research showing sensitivity of active neurons and coherent network activity to electrical stimulation [6,15]. Prior research demonstrated peak sensitivity to stimulation at the theta frequency band [6]. In this study, we used 5 Hz for low frequency stimulation and as the envelope of amplitude-modulation waveform. Keeping the envelope frequency fixed, we studied effect of different carrier frequencies in modulating gamma oscillation in contrast to unmodulated waveforms. Our approach was to systematically contrast the acute effect (2 s, 100 repetitions per slice) of 5 Hz (low), 100 Hz (mid), and 2 kHz (high) frequency sinusoidal unmodulated electric field with 5 Hz amplitude-modulated kHz electric fields with 0.1, 1, or 2 kHz carrier, on

gamma oscillations in hippocampal brain slices. For each waveform a range of electric field amplitudes were tested around an empirical threshold range.

We defined two metrics to quantify gamma power: 1) dynamic modulation, which captures fluctuations in gamma power during stimulation; and 2) static modulation, which captures the average gamma power during stimulation (see Methods). Unless otherwise stated, results are reported as mean ± SEM. Low-frequency 5 Hz sine electric field was applied at intensities of 1, 3 and 5 V/m (Fig. 2B1). There was a monotonic relationship between electric field intensity and dynamic modulation of gamma power, with statistically significant effects for field intensities >1 V/m (3 V/m: dynamic modulation = 1.36 ± 0.01, n = 8, p < 10^−4; 5 V/m: dynamic modulation = 1.65 ± 0.07, n = 8, p < 10^−4) (Fig. 2D2). The enhancement and suppression during each phase of the 5 Hz stimulation was approximately symmetric, such that there was no statistically significant static modulation (n = 8, p = 0.5, one-way ANOVA) (Fig. 2D1, sine 5 Hz).

Stimulation with unmodulated sinusoids at mid (100 Hz) and high frequencies (2 kHz) did not produce statistically significant changes in hippocampal gamma oscillations using intensities effective for low-frequency stimulation (i.e.   5 V/m). Statistically significant steady increases (static modulation) in gamma power were detected using electric field intensities   7 V/m for 100 Hz (7 V/m: static modulation = 1.11 ± 0.06, n = 9, p = 0.0287; 10 V/m: static modulation = 1.14 ± 0.037, n = 9, p < 0.001) (Fig. 2 B.2) and electric field intensities   80 V/m for 2 kHz (80 V/m: static modulation = 1.15 ± 0.07, n = 6, p = 0.006; 100 V/m: static modulation = 1.20 ± 0.01, n = 6, p < 0.001) (Fig. 2 B.3). As tested, 2 kHz stimulation did not change the frequency of peak gamma power, while 100 Hz stimulation shifted ongoing oscillation frequency by ~5 Hz. A shift in oscillation frequency specifically by 100 Hz stimulation is consistent with prior results showing stimulation near the frequency (or near harmonic) of an endogenous oscillation have the lowest threshold to shift the oscillation frequency [6,15,54]. Static modulation increased with increasing electric field intensity (Fig. 2D1) and decreased with increasing stimulation frequency. Using higher frequencies, stronger field intensities were required to produce the same effect (Fig. 2D1). Stimulation with unmodulated sinusoids at frequencies of 100 Hz and 2 kHz did not produce dynamic modulation of oscillations-this result is expected since these waveforms include no low-frequency (e.g. 5 Hz) amplitude modulation.

Stimulation with 5 Hz amplitude-modulated waveforms resulted in dynamic modulation of hippocampal gamma activity at the 5 Hz "beating" frequency (Fig. 2A2). The magnitude of this dynamic modulation of oscillations increased with electric field magnitude and decreased with carrier frequency (Fig. 2D2). 5 Hz amplitude-modulated stimulation produced statistically significant dynamic modulation using electric field intensities   5 V/m for 100 Hz carrier (5 V/m: dynamic modulation = 1.16 ± 0.08, n = 10, p < 0.001; 7 V/m: dynamic modulation = 1.280.12, n = 11, p < 0.001; 10 V/m: dynamic modulation = 1.42 ± 0.14, n = 11, p < 0.001; 15 V/m: dynamic modulation = 1.61 ± 0.06, n = 5, p < 0.001). Electric fields greater than   60 V/m were effective with a 1 kHz carrier (60 V/m: dynamic modulation = 1.33 ± 0.10, n = 8, p < 0.001; 80 V/m: dynamic modulation = 1.68 ± 0.03, n = 7, p < 0.001). Electric fields   80 V/m were effective with a 2 kHz carrier (80 V/m: dynamic modulation = 1.35 ± 0.11, n = 7, p < 0.001; 100 V/m: dynamic modulation = 1.50 ± 0.14,

n = 6, p < 0.001). Amplitude-modulated stimulation with 1 kHz and 2 kHz stimulation did not change the frequency of peak gamma power, while 100 Hz carrier stimulation shifted ongoing oscillation frequency by ~5 Hz.

Stimulation with 5 Hz amplitude-modulated waveforms also produced statistically significant static modulation for intensities 15 V/m for 100 Hz carrier (15 V/m: static modulation = 1.10 ± 0.06, n = 5, p = 0.046), 60 V/m for 1 kHz carrier (60 V/m: static modulation = 1.09 ± 0.09, n = 8, p = 0.048; 80 V/m: static modulation = 1.11 ± 0.09, n = 7, p = 0.014) and 100 V/m for a 2 kHz carrier (100 V/m: static modulation = 1.10 ± 0.01, n = 6, p = 0.032); showing a non-symmetric effect on gamma power modulation. Hippocampal gamma oscillation sensitivity to amplitude-modulated waveforms decreases with increasing carrier frequency; so stronger stimulation intensities are required to modulate gamma activity when higher carrier frequencies are used (Fig. 2D2).

3.3. Computational network model of hippocampal gamma oscillation

It is well known that the sensitivity of transmembrane potentials to sinusoidal electric fields decreases with increasing stimulation frequency [15] which is explained by the membrane time constant [15,23]. In active networks, sensitivity to electric fields is further dependent on network dynamic [6,15,44]. However, the implications of these prior findings to amplitude-modulated kHz electric field have remained unclear. We adapted a previously verified computational network model of hippocampal gamma oscillations. The model used single-compartment excitatory and inhibitory neurons, which were coupled to the external electric field [6]. The computational model provided quantitative predictions for the sensitivity of gamma oscillations to unmodulated and amplitude-modulated stimulation across frequencies. Two key modifications to the prior model were implemented: 1) in addition to fast synaptic inhibition, motivated by typical $GABA_a$ receptors [6,55], we also included a slower $GABA_b$-type inhibitory conductance with higher activation threshold [56,57]; 2) the membrane time constant (τ) was decreased to 1 m s. We further show that these properties are essential to sensitivity and selectivity of temporal interference stimulation.

For low-frequency 5 Hz sine, the model reproduced experimental modulation of hippocampal gamma power (Fig. 2E1, E2, sine) as shown previously [6]. For higher frequency stimulation (both amplitude-modulated and unmodulated), the model captured major features of our in vitro experiments: 1) the inverse relationship between stimulation carrier frequency and the sensitivity of gamma oscillations to stimulation (i.e. much higher electric field magnitude required for high frequency stimulation (Fig. 2E1, E2)); 2) for a given carrier frequency, static modulation and dynamic modulation increased with field magnitude (Fig. 2E1, E2); 3) stimulation with the 100 Hz carrier shifted gamma oscillation frequency, while 1 and 2 kHz carriers did not produce significant change in gamma frequency.

For stimulation with unmodulated mid (100 Hz) and high (2 kHz) frequency electric field, the model also reproduced the specific time course of gamma power modulation in our experiments. There is a rise in gamma power at the onset of stimulation, followed by a decay to steady state, which remains above baseline (Fig. 3B). We only observed increased

gamma power, reflecting the sensitivity of the active network to the depolarizing phase of the sinusoidal electric field waveform. Indeed, the response profile in unmodulated high frequency stimulation is similar to DC depolarizing stimulation [6]. The observed time constant of network adaptation is governed by recruitment of high-threshold inhibitory neurons, which produce slow $GABA_b$ post-synaptic inhibition [56] (Fig. 3A3).

Stimulation of 5 Hz-amplitude-modulated waveforms modulated ongoing hippocampal gamma oscillation at the envelop frequency (5 Hz) as observed in vitro. Notably dynamic modulation due to amplitude-modulated waveforms was greater than the static modulation due to the corresponding unmodulated waveform. In the model this difference depends on the presence of $GABA_b$ synapses, which control the timescale of network adaptation (Fig. 3A1).

Generalized model of network oscillation sensitivity and selectivity to Temporal Interference stimulation.

The above model was built to match experimental data in hippocampal CA3 slices. To generalize the model, we considered how its predictions depend on details of the model's biophysical parameters. Specifically, changes in membrane time constant and GABAergic inhibition (GABA_b), with alterations described relative to the computational network parameters that reproduced hippocampal gamma oscillations ($\tau_m = 1$ ms, $+ GABA_b$, solid blue line, Fig. 3A).

Decreasing the membrane time constant increased the sensitivity of gamma oscillations to both amplitude-modulated and unmodulated kHz electric fields (Fig. 3A1, 3A3; solid red line $\tau_m = 0.4$ ms). Conversely, increasing the membrane time constant led to insensitivity of gamma oscillations to stimulation waveforms in the electric field range tested in experiments (Fig. 3A, $\tau_m = 3$ ms, solid green line). In our model, the single-compartment membrane time constant reflected the most sensitive neuronal element to kHz stimulation. A membrane time constant of 1 m s reproduced our experimental data which is moderately faster than prior simulations of gamma oscillations ($\tau_m = 3$–10 m s [45,55,58]) and the resting state somatic polarization time constant by electric fields ($\tau_m \sim 20$ m s [6,15]). This finding has direct implications for the neuronal element targeted by interferential stimulation, namely axons [26,59].

Spiking activity in the model suggested a slight increase in unit activity even at an electric field intensity below the thresholds for modulating network of gamma oscillations (Fig. 3A2). It is expected that (the most sensitive) individual neurons will respond to electric field before changes in network power exceed a threshold [6].

Removing GABA_b-mediated inhibition decreased dynamic modulation in response to amplitude-modulated waveforms, while increasing static modulation in response to unmodulated sinusoidal electric fields (solid lines (+GABA_b), dashed lines (−GABA_b); Fig. 3A). The GABA_b synapses are therefore critical for the network to exhibit sensitivity and selectivity for amplitude-modulated waveforms.

Finally, we determined how sensitivity and selectivity to temporal interference stimulation across the brain are governed by cellular and network biophysics (Fig. 3B). To do so we assumed a generic neural circuit, which reoccurs throughout the brain (i.e. at each voxel), simulated with the experimentally validated model described above. Of course, not all brain regions are identical, but such an approach allows a principled analysis of the parameters governing sensitivity/selectivity of the brain to temporal interference stimulation.

The electric fields generated in each brain region ($2 \times 2 \times 1$ mm voxel) of the temporal interference current flow model was used as the input (I_{stim}) in the network model of gamma oscillations. The electric field varied in both peak intensity and the degree of amplitude-modulation across regions, which produces a mix of static and dynamic neuromodulation at each brain region (e.g. exemplary regions A, B, C). Mapping of static and dynamic modulation in each region is then represented using thresholds derived from experimental hippocampal recordings. In these series only the cellular and network biophysics are varied, with the applied stimulation current (I) selected to demonstrate sensitivity and selectivity (Fig. 3C).

To test the robustness of the multiscale model and to identify which features govern sensitivity and selectivity, we varied parameters that were found to be critical for determining static and dynamic neural modulation in the network model (i.e. τ_m, $GABA_b$). A faster membrane time constant reduced the minimum stimulation current required to modulate oscillations in deep regions (i.e. increased sensitivity to temporal interference stimulation; Fig. 3C). However, even for the most sensitive parameter choice (Fig. 3C1, $\tau_m = 0.4$ ms), this threshold stimulation current was still much higher than conventional tACS (i.e. 83 mA vs 2 mA).

Removing $GABA_b$ inhibition reduced hot spots of dynamic modulation in (target) deep brain regions, while increasing static modulation in overlying cortex (Fig. 3C1–3C3). Therefore, $GABA_b$ inhibition improved selectivity for deep brain regions. However, the model predicted that dynamic modulation in deep brain regions (Fig. 3C, top row) was generally associated with static modulation of cortical areas (Fig. 3C, bottom row). This indicates that selectivity is rather limited regardless of parameter choices.

4.   Discussion

Temporal interference stimulation has been promoted as a tool to selectively modulate neural activity in deep brain regions [1]. The ability of temporal interference stimulation to achieve such selectivity depends on 1) the relative magnitude of amplitude-modulated kHz electric fields (in deep brain region) as compared to the unmodulated kHz electric field (in cortex), and 2) the sensitivity of regional neural networks to amplitude-modulated kHz electric field in contrast to unmodulated kHz waveforms. With regards to the electric field magnitude during temporal interference stimulation, this can be predicted with validated finite element head models (Fig. 1A). With regards to network sensitivity, here we calibrated the dose-response to amplitude-modulated kHz and unmodulated kHz waveforms in a canonical model of hippocampal gamma oscillations (Fig. 2). We showed how cellular and network biophysics, namely the time constants of axonal membranes and GABAergic

inhibition, can explain (Fig. 2) and generalize (Fig. 3) both sensitivity and selectivity to temporal interference stimulation. Integrating experimentally verified current flow and network models, we could make predictions about the ability of temporal interference stimulation to selectively target deep brain regions.

Starting with hippocampal gamma oscillations, we showed an amplitude-modulated kHz (1 kHz modulated at 5 Hz) electric field of ~60 V/m is required for statistically significant dynamic modulation of oscillations (Fig. 2D2), while an unmodulated kHz electric field of the same intensity (~60 V/m) is required to produce static modulation (Fig. 3A3). Assuming these biophysics are uniform across the brain, selectivity therefore requires that the amplitude-modulated kHz electric field magnitude in deep brain regions be greater than ~60 V/m, while the unmodulated kHz electric field in the cortex is less than ~60 V/m. Is this achievable with temporal interference stimulation? With a basic dual bipolar electrode configuration, producing 60 V/m in deep brain regions required ~167 mA on the scalp (Fig. 1A3), corresponding to a peak unmodulated electric field of ~80 V/m at the cortex (Fig. 1A2). This result makes it unlikely for temporal interference stimulation to produce dynamic modulation with amplitude-modulated kHz electric field in deep brain regions without also producing static modulation of the overlying cortex with unmodulated kHz electric field. This prediction holds across a range of neuronal and network biophysics, under the assumption that they are uniform across the brain (Fig. 3C). However, selective deep brain stimulation by temporal interference stimulation derives from: 1) use of more sophisticated electrode montages [3,20]; 2) cellular or network features special to deep brain regions; or 3) impact (value) of dynamic oscillations in deep brain regions versus static modulation at superficial cortex. Ascendant to any approach to temporal interference stimulation, we showed that the sensitivity (applied current required) and selectivity (responsiveness to amplitude-modulated verse unmodulated electric) of the brain to temporal interference stimulation was governed by neural-compartment and network-oscillation features identified here.

What explains the sensitivity of the brain to temporal interference? Amplitude-modulated kHz stimulation has frequency content around the carrier frequency, not at the beat frequency, such that the low-pass filtering properties of neuronal membranes [15,23] will attenuate amplitude-modulated kHz similarly to unmodulated kHz [2,18]. Whereas prior neuron models of low-frequency stimulation (tDCS, tACS) considered polarization of somatic [6,18] or dendritic compartments [25,60–62], here we considered axonal polarization. Axons not only have the highest sensitivity to stimulation (polarization coupling constant 4× of somas [59]) they also have the fastest time constants. A membrane time constant not exceeding 1 m s is pivotal to sensitivity to kHz carriers (Fig. 3A) implicating axons as the temporal interference stimulated neuronal element. Active networks provide additional amplification by effectively increasing the polarization coupling constant [6,63], and through non-linear network responses [12,13,64,65]. Characterizing what determines the sensitivity of deep brain regions to amplitude-modulated kHz stimulation should consider how axons are polarized [66,67] as well as network amplification factors.

With regard to selectivity, we note that even conventional tES easily reaches deep brain structures [11,14,68,69] with some deep selectivity achievable with High-Definition (HD)

optimization [3,20]. Temporal interference stimulation offers possibilities to further improve selectivity, but this is subject to constraints on current flow patterns [3,4] (Fig. 1A) and the potency of amplitude-modulated electric fields compared to unmodulated electric fields [2]. Here this potency is largely determined by the magnitude and time constant of a network homeostatic adaptation mechanism. For unmodulated kHz electric fields (e.g. in cortex), this adaptation *suppresses* the degree of static modulation. For amplitude-modulated kHz electric fields (e.g. in deep brain), this adaptation *boosts* the degree of dynamic modulation. Here we attribute this adaptation mechanism to $GABA_b$ synapses [56], though other cellular and network adaptation mechanisms exist, including short term presynaptic plasticity with short term facilitation and depression dynamics [70,71], spike-frequency adaptation through modulating ionic currents including voltage-gated potassium, calcium-gated potassium channels and slow recovery from inactivation of fast sodium currents [72]. Regardless of mechanism, we show only adaptation mechanisms on a timescale faster that the amplitude-modulation "beat" frequency should enhance dynamic modulation and selectivity.

Does a brain slice model capture neuronal transduction mechanisms for temporal interference stimulation? Even ad hoc (not optimized [3]) temporal interference stimulation electrode placements result in deep regions where the electric fields produced by each electrode pair in direction of interest are aligned and with similar magnitude, generating approximately full amplitude modulated waveform (~AM (100%)) (Fig. 1A [1,4]). Unmodulated electric fields in the superficial cortex are determined by the proximal electrode pair. In either case, neuronal compartments oriented along the electric field are maximally polarized. The brain slice preparation thus supports direct reproduction of electric fields most relevant to temporal interference stimulation [1–4,19,31,32] (Fig. 2). In intermediate brain regions with distinct electric field contributions from each electrode pair, the resultant electric field is partially amplitude modulated, with maximal polarization of aligned neuronal elements (Fig. 3). In cases where electric field vectors are not parallel, the electric field rotates at the carrier frequency, however the electric field waveform along any neuronal compartment is unchanged.

Cellular and networks biophysics are not uniform across the brain, and moreover would change with brain state [73] and disease [31]. Similarly, divergent results across animal studies (e.g. high selectivity of amplitude-modulated kHz [1]; or low sensitivity to tACS [74]) may be explained by variability in these governing parameters. A litany of mechanisms known to influence sensitivity to low-intensity electric fields, including dendrite polarization of excitatory or inhibitory neurons [23,60], synaptic terminal modulation [67,75], stochastic resonance [76], and stimulation of glia [77,78] or endothelial cells [79,80], could be speculated to impact temporal interference stimulation, but were not needed to model our results (Fig. 2). Mechanisms relevant for high-intensity electric fields such as ion accumulation [81], fiber block [82–84], transverse axonal polarization [85], asynchronous firing [86] and/or heating [87] were not required to explain our results.

We show that selective stimulation of deep brain regions derives from phasic modulation of neuronal oscillation with dynamic adapting faster than the "beat" frequency of temporal interference stimulation. An outstanding question for effectiveness of temporal interference is how much current intensity at the scalp is the required in human experiments?

Oscillations provide some amplification, but sensitivity is ultimately throttled by membrane constant (e.g. > 80 mA current even for 0.4 m s time constant; Fig. 3C). As emphasized throughout this paper, these quantitative predictions are limited by any biophysical features absent from our models. Effective temporal interference with intensities comparable to conventional tACS (~2 mA) would require a transduction mechanism with an especially fast time constant - that is absent in acute rodent brain slice oscillations (Fig. 2). Alternatively, meaningful changes in cognition could derive through modulating a limited number of hyper-responsive neurons without impacting network dynamic. The intention of temporal interference stimulation is not necessarily linked to modulation of oscillations; use of network oscillations here reflects long-standing research that active neurons are more sensitive to electric fields then quiescent cells [19,88–90], and coherent network activity more sensitive still [6,49,91–93]. We would have detected any activation (pacing). Notwithstanding limitations, we show that the cellular mechanisms of temporal interference stimulation of the brain, including threshold currents for human experiments, can be addressed through the sensitivity and selectivity of neuronal oscillations.

Declaration of competing interest

References

[1]. Grossman N, Bono D, Dedic N, Kodandaramaiah SB, Rudenko A, Suk HJ, et al. Noninvasive deep brain stimulation via temporally interfering electric fields. Cell 2017;169(6):1029–41. e16. [PubMed: 28575667]

[2]. Dmochowski J, Bikson M. Noninvasive neuromodulation goes deep. Cell 2017;169(6):977–8. [PubMed: 28575675]

[3]. Huang Y, Parra LC. Can transcranial electric stimulation with multiple electrodes reach deep targets? Brain Stimul 2019;12(1):30–40. [PubMed: 30297323]

[4]. Rampersad S, Roig-Solvas B, Yarossi M, Kulkarni PP, Santarnecchi E, Dorval AD, et al. Prospects for transcranial temporal interference stimulation in humans: a computational study. bioRxiv 2019:602102.

[5]. Frohlich F, McCormick DA. Endogenous electric fields may guide neocortical network activity. Neuron 2010;67(1):129–43. [PubMed: 20624597]

[6]. Reato D, Rahman A, Bikson M, Parra LC. Low-intensity electrical stimulation affects network dynamics by modulating population rate and spike timing. J Neurosci 2010;30(45):15067–79. [PubMed: 21068312]

[7]. Ozen S, Sirota A, Belluscio MA, Anastassiou CA, Stark E, Koch C, et al. Transcranial electric stimulation entrains cortical neuronal populations in rats. J Neurosci 2010;30(34):11476–85. [PubMed: 20739569]

[8]. Basar E Brain oscillations in neuropsychiatric disease. Dialogues Clin Neurosci 2013;15(3):291–300. [PubMed: 24174901]

[9]. Kahana MJ. The cognitive correlates of human brain oscillations. J Neurosci 2006;26(6):1669–72. [PubMed: 16467513]

[10]. Pevzner A, Izadi A, Lee DJ, Shahlaie K, Gurkoff GG. Making waves in the brain: what are oscillations, and why modulating them makes sense for brain injury. Front Syst Neurosci 2016;10:30. [PubMed: 27092062]

[11]. Huang Y, Liu AA, Lafon B, Friedman D, Dayan M, Wang X, et al. Measurements and models of electric fields in the in vivo human brain during transcranial electric stimulation. Elife 2017;6.

[12]. Kar K, Duijnhouwer J, Krekelberg B. Transcranial alternating current stimulation attenuates neuronal adaptation. J Neurosci 2017;37(9):2325–35. [PubMed: 28137971]

[13]. Schmidt SL, Iyengar AK, Foulser AA, Boyle MR, Frohlich F. Endogenous cortical oscillations constrain neuromodulation by weak electric fields. Brain Stimul 2014;7(6):878–89. [PubMed: 25129402]

[14]. Krause MR, Vieira PG, Csorba BA, Pilly PK, Pack CC. Transcranial alternating current stimulation entrains single-neuron activity in the primate brain. Proc Natl Acad Sci U S A 2019;116(12):5747–55. [PubMed: 30833389]

[15]. Deans JK, Powell AD, Jefferys JG. Sensitivity of coherent oscillations in rat hippocampus to AC electric fields. J Physiol 2007;583(Pt 2):555–65. [PubMed: 17599962]

[16]. Reato D, Rahman A, Bikson M, Parra LC. Effects of weak transcranial alternating current stimulation on brain activity-a review of known mechanisms from animal studies. Front Hum Neurosci 2013;7:687. [PubMed: 24167483]

[17]. Couto J, Grill WM. Kilohertz frequency deep brain stimulation is ineffective at regularizing the firing of model thalamic neurons. Front Comput Neurosci 2016;10:22. [PubMed: 27014047]

[18]. Negahbani E, Kasten FH, Herrmann CS, Fröhlich F. Targeting alpha-band oscillations in a cortical model with amplitude-modulated high-frequency transcranial electric stimulation. Neuroimage 2018;173:3–12. [PubMed: 29427848]

[19]. Howell B, McIntyre CC. Feasibility of interferential and pulsed transcranial electrical stimulation for neuromodulation at the human scale. Neuromodulation 2020.

[20]. Dmochowski JP, Datta A, Bikson M, Su Y, Parra LC. Optimized multi-electrode stimulation increases focality and intensity at target. J Neural Eng 2011;8(4): 046011. [PubMed: 21659696]

[21]. Chaieb L, Antal A, Paulus W. Transcranial alternating current stimulation in the low kHz range increases motor cortex excitability. Restor Neurol Neurosci 2011;29(3):167–75. [PubMed: 21586823]

[22]. Kunz P, Antal A, Hewitt M, Neef A, Opitz A, Paulus W. 5 kHz transcranial alternating current stimulation: lack of cortical excitability changes when grouped in a theta burst pattern. Front Hum Neurosci 2016;10:683. [PubMed: 28119589]

[23]. Bikson M, Inoue M, Akiyama H, Deans JK, Fox JE, Miyakawa H, et al. Effects of uniform extracellular DC electric fields on excitability in rat hippocampal slices in vitro. J Physiol 2004;557(Pt 1):175–90. [PubMed: 14978199]

[24]. Bawin S, Sheppard AR, Mahoney MD, Adey WR. Influences of sinusoidal electric fields on excitability in the rat hippocampal slice. Brain Res 1984;323(2):227–37. [PubMed: 6098340]

[25]. Maeda K, Maruyama R, Nagae T, Inoue M, Aonishi T, Miyakawa H. Weak sinusoidal electric fields entrain spontaneous Ca transients in the dendritic tufts of CA1 pyramidal cells in rat hippocampal slice preparations. PLoS One 2015;10(3):e0122263. [PubMed: 25811836]

[26]. Rahman A, Reato D, Arlotti M, Gasca F, Datta A, Parra LC, et al. Cellular effects of acute direct current stimulation: somatic and synaptic terminal effects. J Physiol 2013;591(10):2563–78. [PubMed: 23478132]

[27]. Fisahn A, Pike FG, Buhl EH, Paulsen O. Cholinergic induction of network oscillations at 40 Hz in the hippocampus in vitro. Nature 1998;394(6689): 186–9. [PubMed: 9671302]

[28]. Kasten FH, Negahbani E, Frohlich F, Herrmann CS. Non-linear transfer characteristics of stimulation and recording hardware account for spurious low-frequency artifacts during amplitude modulated transcranial alternating current stimulation (AM-tACS). Neuroimage 2018;179:134–43. [PubMed: 29860086]

[29]. FallahRad M, Zannou AL, Khadka N, Prescott SA, Ratte S, Zhang T, et al. Electrophysiology equipment for reliable study of kHz electrical stimulation. J Physiol 2019;597(8):2131–7. [PubMed: 30816558]

[30]. Lesperance LS, Lankarany M, Zhang TC, Esteller R, Ratte S, Prescott SA. Artifactual hyperpolarization during extracellular electrical stimulation: proposed mechanism of high-rate neuromodulation disproved. Brain Stimul 2018;11(3):582–91. [PubMed: 29289565]

[31]. Grossman N, Okun MS, Boyden ES. Translating temporal interference brain stimulation to treat neurological and psychiatric conditions. JAMA Neurol 2018;75(11):1307–8. [PubMed: 30264149]

[32]. Cao J, Grover P. STIMULUS: noninvasive dynamic patterns of neurostimulation using spatio-temporal interference. IEEE Trans Biomed Eng 2020;67(3): 726–37. [PubMed: 31150335]

[33]. Bikson M, Dmochowski J, Rahman A. The "quasi-uniform" assumption in animal and computational models of non-invasive electrical stimulation. Brain Stimul 2013;6(4):704–5. [PubMed: 23290681]

[34]. Khadka N, Truong DQ, Williams P, Martin JH, Bikson M. The quasi-uniform assumption for spinal cord stimulation translational research. J Neurosci Methods 2019;328:108446. [PubMed: 31589892]

[35]. Bikson M, Truong DQ, Mourdoukoutas AP, Aboseria M, Khadka N, Adair D, et al. Modeling sequence and quasi-uniform assumption in computational neurostimulation. Prog Brain Res 2015;222:1–23. [PubMed: 26541374]

[36]. Durand DM, Bikson M. Suppression and control of epileptiform activity by electrical stimulation: a review. Proc IEEE 2001;89(7):1065–82.

[37]. Ghai RS, Bikson M, Durand DM. Effects of applied electric fields on low-calcium epileptiform activity in the CA1 region of rat hippocampal slices. J Neurophysiol 2000;84(1):274–80. [PubMed: 10899202]

[38]. Team RC. R version 3.5. 1 (Feather Spray): a language and environment for statistical computing. R Foundation for Statistical Computing, Vienna, Austria URL **Error! Hyperlink reference not valid.**.

[39]. Bates D, Mächler M, Bolker B, Walker S. Fitting linear mixed-effects models using lme4. arXiv. org. preprint, 10; 2014.

[40]. Bossetti CA, Birdno MJ, Grill WM. Analysis of the quasi-static approximation for calculating potentials generated by neural stimulation. J Neural Eng 2007;5(1):44. [PubMed: 18310810]

[41]. Huang Y, Parra LC. Can transcranial electric stimulation with multiple electrodes reach deep targets? Brain Stimul 2019;12(1):30–40. [PubMed: 30297323]

[42]. Naud R, Marcille N, Clopath C, Gerstner W. Firing patterns in the adaptive exponential integrate-and-fire model. Biol Cybern 2008;99(4–5):335–47. [PubMed: 19011922]

[43]. Traub RD, Miles R. Multiple modes of neuronal population activity emerge after modifying specific synapses in a model of the CA3 region of the hippocampus. Ann N Y Acad Sci 1991;627(1):277–90. [PubMed: 1883139]

[44]. Economo MN, White JA. Membrane properties and the balance between excitation and inhibition control gamma-frequency oscillations arising from feedback inhibition. PLoS Comput Biol 2012;8(1):e1002354. [PubMed: 22275859]

[45]. Atallah BV, Scanziani M. Instantaneous modulation of gamma oscillation frequency by balancing excitation with inhibition. Neuron 2009;62(4): 566–77. [PubMed: 19477157]

[46]. Traub RD, Jefferys J, Miles R, Whittington MA, Tóth K. A branching dendritic model of a rodent CA3 pyramidal neurone. J Physiol 1994;481(1):79–95. [PubMed: 7853251]

[47]. Lafon B, Rahman A, Bikson M, Parra LC. Direct current stimulation alters neuronal input/output function. Brain Stimul 2017;10(1):36–45. [PubMed: 27717601]

[48]. Ali MM, Sellers KK, Frohlich F. Transcranial alternating current stimulation modulates large-scale cortical network activity by network resonance. J Neurosci 2013;33(27):11262–75. [PubMed: 23825429]

[49]. Frohlich F. Experiments and models of cortical oscillations as a target for noninvasive brain stimulation. Prog Brain Res 2015;222:41–73. [PubMed: 26541376]

[50]. Radman T, Ramos RL, Brumberg JC, Bikson M. Role of cortical cell type and morphology in subthreshold and suprathreshold uniform electric field stimulation in vitro. Brain Stimul 2009;2(4):215–28. 28.e1–3. [PubMed: 20161507]

[51]. Hajos N, Palhalmi J, Mann EO, Nemeth B, Paulsen O, Freund TF. Spike timing of distinct types of GABAergic interneuron during hippocampal gamma oscillations in vitro. J Neurosci 2004;24(41):9127–37. [PubMed: 15483131]

[52]. Oren I, Mann EO, Paulsen O, Hajos N. Synaptic currents in anatomically identified CA3 neurons during hippocampal gamma oscillations in vitro. J Neurosci 2006;26(39):9923–34. [PubMed: 17005856]

[53]. Datta A, Zhou X, Su Y, Parra LC, Bikson M. Validation of finite element model of transcranial electrical stimulation using scalp potentials: implications for clinical dose. J Neural Eng 2013;10(3):036018. [PubMed: 23649036]

[54]. Fröhlich F. Endogenous and exogenous electric fields as modifiers of brain activity: rational design of noninvasive brain stimulation with transcranial alternating current stimulation. Dialogues Clin Neurosci 2014;16(1):93. [PubMed: 24733974]

[55]. Karbowski J, Kopell N. Multispikes and synchronization in a large neural network with temporal delays. Neural Comput 2000;12(7):1573–606. [PubMed: 10935919]

[56]. Brown JT, Davies CH, Randall AD. Synaptic activation of GABAB receptors regulates neuronal network activity and entrainment. Eur J Neurosci 2007;25(10):2982–90. [PubMed: 17561812]

[57]. Newberry NR, Nicoll RA. A bicuculline-resistant inhibitory post-synaptic potential in rat hippocampal pyramidal cells in vitro. J Physiol 1984;348: 239–54. [PubMed: 6716285]

[58]. Börgers C, Epstein S, Kopell NJ. Background gamma rhythmicity and attention in cortical local circuits: a computational study. Proc Natl Acad Sci U S A 2005;102(19):7002–7. [PubMed: 15870189]

[59]. Chakraborty D, Truong DQ, Bikson M, Kaphzan H. Neuromodulation of axon terminals. Cerebr Cortex 2017;28(8):2786–94.

[60]. Kronberg G, Bridi M, Abel T, Bikson M, Parra LC. Direct current stimulation modulates LTP and LTD: activity dependence and dendritic effects. Brain Stimul 2017;10(1):51–8. [PubMed: 28104085]

[61]. Rahman A, Lafon B, Parra LC, Bikson M. Direct current stimulation boosts synaptic gain and cooperativity in vitro. J Physiol 2017;595(11):3535–47. [PubMed: 28436038]

[62]. Kronberg G, Rahman A, Sharma M, Bikson M, Parra LC. Direct current stimulation boosts hebbian plasticity in vitro. Brain Stimul 2019.

[63]. Toloza EHS, Negahbani E, Frohlich F. Ih interacts with somato-dendritic structure to determine frequency response to weak alternating electric field stimulation. J Neurophysiol 2018;119(3):1029–36. [PubMed: 29187553]

[64]. Reato D, Bikson M, Parra LC. Lasting modulation of in vitro oscillatory activity with weak direct current stimulation. J Neurophysiol 2015;113(5):1334–41. [PubMed: 25505103]

[65]. Cabral-Calderin Y, Williams KA, Opitz A, Dechent P, Wilke M. Transcranial alternating current stimulation modulates spontaneous low frequency fluctuations as measured with fMRI. Neuroimage 2016;141:88–107. [PubMed: 27393419]

[66]. Arlotti M, Rahman A, Minhas P, Bikson M. Axon terminal polarization induced by weak uniform DC electric fields: a modeling study. Conf Proc IEEE Eng Med Biol Soc 2012:4575–8.

[67]. Rahman A, Reato D, Arlotti M, Gasca F, Datta A, Parra LC, et al. Cellular effects of acute direct current stimulation: somatic and synaptic terminal effects. J Physiol 2013;591(10):2563–78. [PubMed: 23478132]

[68]. Dasilva AF, Mendonca ME, Zaghi S, Lopes M, Dossantos MF, Spierings EL, et al. tDCS-induced analgesia and electrical fields in pain-related neural networks in chronic migraine. Headache 2012;52(8):1283–95. [PubMed: 22512348]

[69]. Opitz A, Falchier A, Yan CG, Yeagle EM, Linn GS, Megevand P, et al. Spatio-temporal structure of intracranial electric fields induced by transcranial electric stimulation in humans and nonhuman primates. Sci Rep 2016;6: 31236. [PubMed: 27535462]

[70]. Varela JA, Sen K, Gibson J, Fost J, Abbott LF, Nelson SB. A quantitative description of short-term plasticity at excitatory synapses in layer 2/3 of rat primary visual cortex. J Neurosci 1997;17(20):7926–40. [PubMed: 9315911]

[71]. Zhang C, Peskin CS. Improved signaling as a result of randomness in synaptic vesicle release. Proc Natl Acad Sci U S A 2015;112(48):14954–9. [PubMed: 26627245]

[72]. Benda J, Herz AV. A universal model for spike-frequency adaptation. Neural Comput 2003;15(11):2523–64. [PubMed: 14577853]

[73]. Smitha KA, Akhil Raja K, Arun KM, Rajesh PG, Thomas B, Kapilamoorthy TR, et al. Resting state fMRI: a review on methods in resting state connectivity analysis and resting state networks. NeuroRadiol J 2017;30(4):305–17. [PubMed: 28353416]

[74]. Lafon B, Henin S, Huang Y, Friedman D, Melloni L, Thesen T, et al. Low frequency transcranial electrical stimulation does not entrain sleep rhythms measured by human intracranial recordings. Nat Commun 2017;8(1):1199. [PubMed: 29084960]

[75]. Kabakov AY, Muller PA, Pascual-Leone A, Jensen FE, Rotenberg A. Contribution of axonal orientation to pathway-dependent modulation of excitatory transmission by direct current stimulation in isolated rat hippocampus. J Neurophysiol 2012;107(7):1881–9. [PubMed: 22219028]

[76]. Stacey WC, Durand DM. Stochastic resonance improves signal detection in hippocampal CA1 neurons. J Neurophysiol 2000;83(3):1394–402. [PubMed: 10712466]

[77]. Mishima T, Nagai T, Yahagi K, Akther S, Oe Y, Monai H, et al. Transcranial direct current stimulation (tDCS) induces adrenergic receptor-dependent microglial morphological changes in mice. eNeuro 2019;6(5).

[78]. Monai H, Ohkura M, Tanaka M, Oe Y, Konno A, Hirai H, et al. Calcium imaging reveals glial involvement in transcranial direct current stimulation-induced plasticity in mouse brain. Nat Commun 2016;7:11100. [PubMed: 27000523]

[79]. Cancel LM, Arias K, Bikson M, Tarbell JM. Direct current stimulation of endothelial monolayers induces a transient and reversible increase in transport due to the electroosmotic effect. Sci Rep 2018;8(1):9265. [PubMed: 29915178]

[80]. Shin DW, Fan J, Luu E, Khalid W, Xia Y, Khadka N, et al. In vivo modulation of the blood-brain barrier permeability by transcranial direct current stimulation (tDCS). Ann Biomed Eng 2020;48(4):1256–70. [PubMed: 31916126]

[81]. Bikson M, Lian J, Hahn PJ, Stacey WC, Sciortino C, Durand DM. Suppression of epileptiform activity by high frequency sinusoidal fields in rat hippocampal slices. J Physiol 2001;531(Pt 1):181–91. [PubMed: 11179402]

[82]. Patel YA, Butera RJ. Differential fiber-specific block of nerve conduction in mammalian peripheral nerves using kilohertz electrical stimulation. J Neurophysiol 2015;113(10):3923–9. [PubMed: 25878155]

[83]. Kilgore KL, Bhadra N. Reversible nerve conduction block using kilohertz frequency alternating current. Neuromodulation 2014;17(3):242–54. discussion 54–5. [PubMed: 23924075]

[84]. Vrabec TL, Eggers TE, Foldes EL, Ackermann DM, Kilgore KL, Bhadra N. Reduction of the onset response in kilohertz frequency alternating current nerve block with amplitude ramps from non-zero amplitudes. J NeuroEng Rehabil 2019;16(1):80. [PubMed: 31253152]

[85]. Wang B, Aberra AS, Grill WM, Peterchev AV. Modified cable equation incorporating transverse polarization of neuronal membranes for accurate coupling of electric fields. J Neural Eng 2018;15(2):026003. [PubMed: 29363622]

[86]. Crosby ND, Janik JJ, Grill WM. Modulation of activity and conduction in single dorsal column axons by kilohertz-frequency spinal cord stimulation. J Neurophysiol 2017;117(1):136–47. [PubMed: 27760823]

[87]. Zannou AL, Khadka N, Truong DQ, Zhang T, Esteller R, Hershey B, et al. Temperature increases by kilohertz frequency spinal cord stimulation. Brain Stimul 2019;12(1):62–72. [PubMed: 30482674]

[88]. Radman T, Su Y, An JH, Parra LC, Bikson M. Spike timing amplifies the effect of electric fields on neurons: implications for endogenous field effects. J Neurosci 2007;27(11):3030–6. [PubMed: 17360926]

[89]. Birdno MJ, Tang W, Dostrovsky JO, Hutchison WD, Grill WM. Response of human thalamic neurons to high-frequency stimulation. PLoS One 2014;9(5): e96026. [PubMed: 24804767]

[90]. Stacey WC, Durand DM. Synaptic noise improves detection of subthreshold signals in hippocampal CA1 neurons. J Neurophysiol 2001;86(3):1104–12. [PubMed: 11535661]

[91]. Stacey WC, Durand DM. Noise and coupling affect signal detection and bursting in a simulated physiological neural network. J Neurophysiol 2002;88(5):2598–611. [PubMed: 12424297]

[92]. Francis JT, Gluckman BJ, Schiff SJ. Sensitivity of neurons to weak electric fields. J Neurosci 2003;23(19):7255–61. [PubMed: 12917358]

[93]. Liu A, Voroslakos M, Kronberg G, Henin S, Krause MR, Huang Y, et al. Immediate neurophysiological effects of transcranial electrical stimulation. Nat Commun 2018;9(1):5092. [PubMed: 30504921]
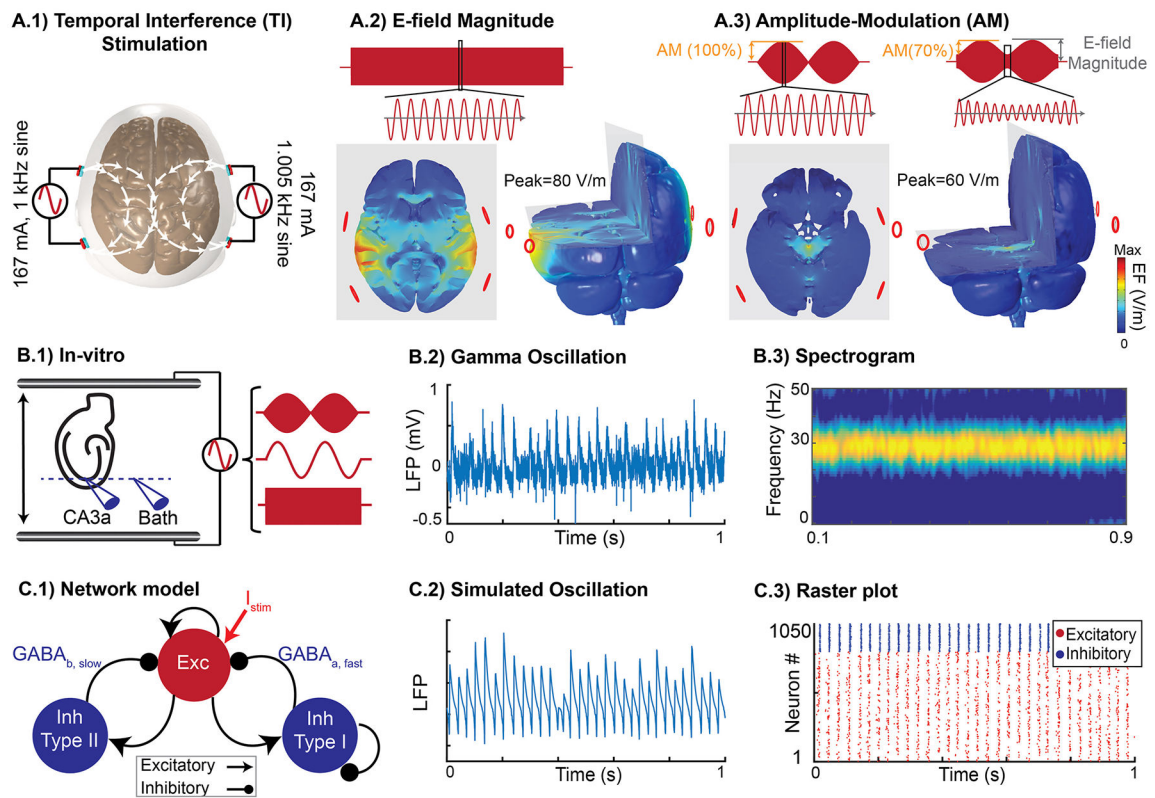
Fig. 1. Experimental and computational approaches.

(A) Computational current-flow model. A.1, Temporal Interference (TI) stimulation via two pairs of electrodes on scalp. Current flows between FT7 and P7 on the left and between FT8 and P8 on the right hemisphere. A.2 Spatial distribution of electric field magnitude in posterior/anterior direction across brain. A.3, Spatial distribution of amplitude-modulation across the brain in posterior/anterior direction. **(B)** Rodent in vitro model of gamma oscillations. B.1, Experimental setup: spatially uniform electric field was applied across hippocampal slice in an interface chamber. Recording of gamma oscillation in CA3a region relative to an iso-potential electrode in the bath. B.2 and B.3, Gamma oscillation induced by 20 μM carbachol in vitro and its stability in power and frequency. **(C)** Computational model of gamma oscillations. C.1, The network model has excitatory and inhibitory neurons (1050 neurons, 800 excitatory) that are sparsely connected with varied synaptic weights. C.2, Simulated gamma oscillation in the network model by averaging postsynaptic currents across the network. C.3, Raster-plot representing the firing activity of excitatory (red) and inhibitory (blue) neurons during induced gamma oscillation.
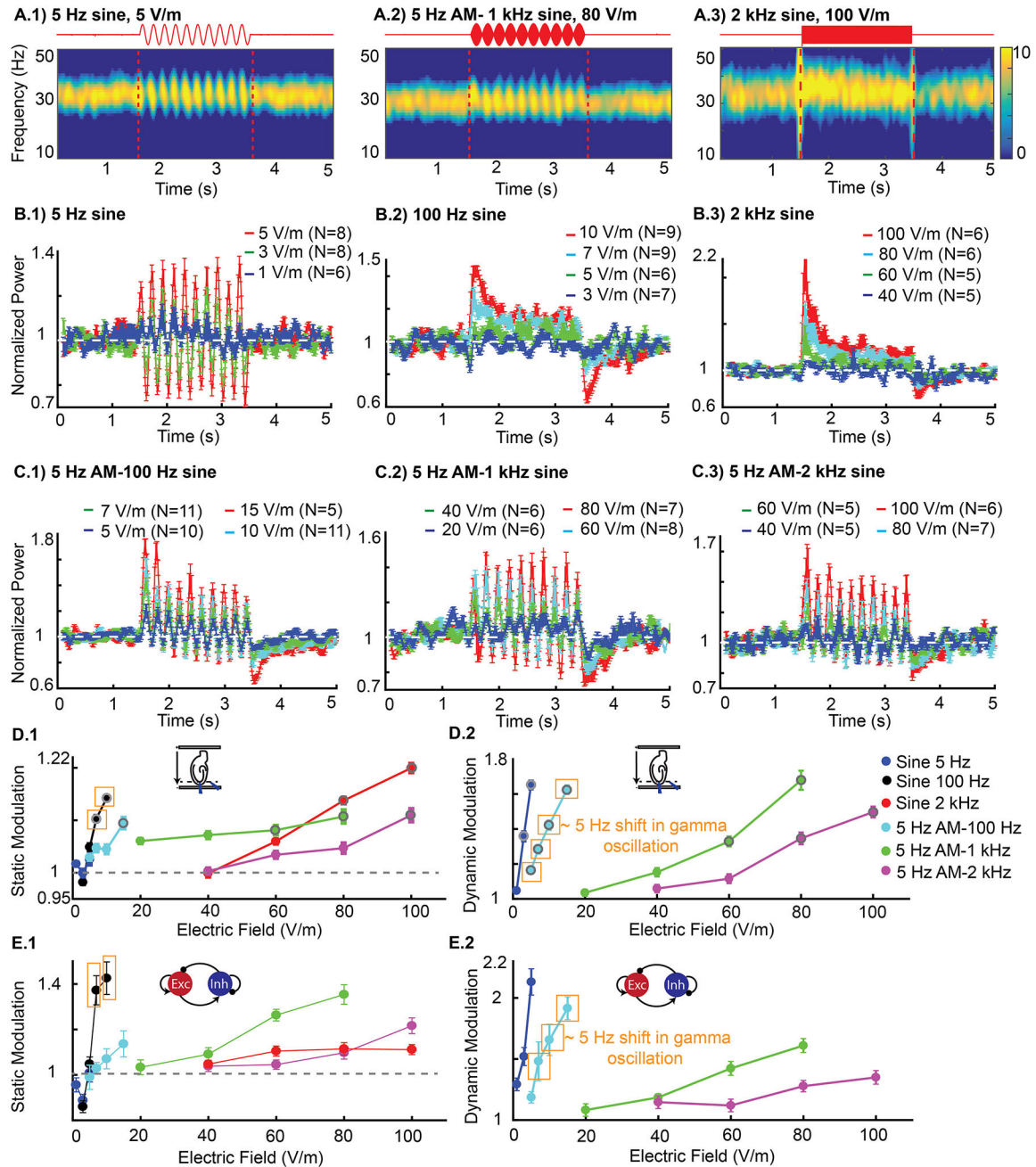
Fig. 2.

Changes in hippocampal gamma oscillation during application of Amplitude-Modulated high-frequency field as well as low, mid and high-frequency (unmodulated) sinusoidal waveforms in vitro. **(A)** Mean spectrogram of oscillation (in dB) for 2 s of stimulation (between 1.5 and 3.5 s) using 5 Hz, 5 V/m sine waveform (A.1), Amplitude-Modulated (AM) waveform, 5 Hz AM-1 kHz sine, 80 V/m (A.2), 2 kHz sine waveform, 100 V/m (A.3). **(B)** Mean (±SEM) of normalized power across slices for different intensities in 5 Hz sine (B.1), 100 Hz sine (B.2), 2 kHz sine (B.3). **(C)** Mean (±SEM) of normalized power across slices for different intensities in amplitude-modulated waveform with 5 Hz envelop and

100 Hz carrier frequency (C.1), 1 kHz carrier frequency (C.2) and 2 kHz carrier frequency (C.3). **(D)** Modulation of gamma power in hippocampal in vitro experiments. D.1) Mean (±SEM) of static modulation of power during stimulation in *in vitro* experiment measured as mean power modulation during 1 s of stimulation relative to baseline. D.2) Mean (±SEM) of dynamic modulation. In 5 Hz sine stimulation, dynamic modulation calculated as power ratio between interval of positive and negative field and in amplitude-modulated waveforms dynamic modulation is quantified as a ratio of peak (>50% of peak field intensity) to trough (<50% of peak field intensity). Error bars indicate standard error of mean. N, number of slices. Grey ring indicates statistically significant modulation relative to baseline, $p < 0.05$; significance was calculated via one-way ANOVA with Tukey post-hoc test. Yellow boxes indicate ~5 Hz shift in peak gamma frequency during 100 Hz stimulation (modulated and unmodulated)**. (E)** Modulation of power during stimulation in computational network model.
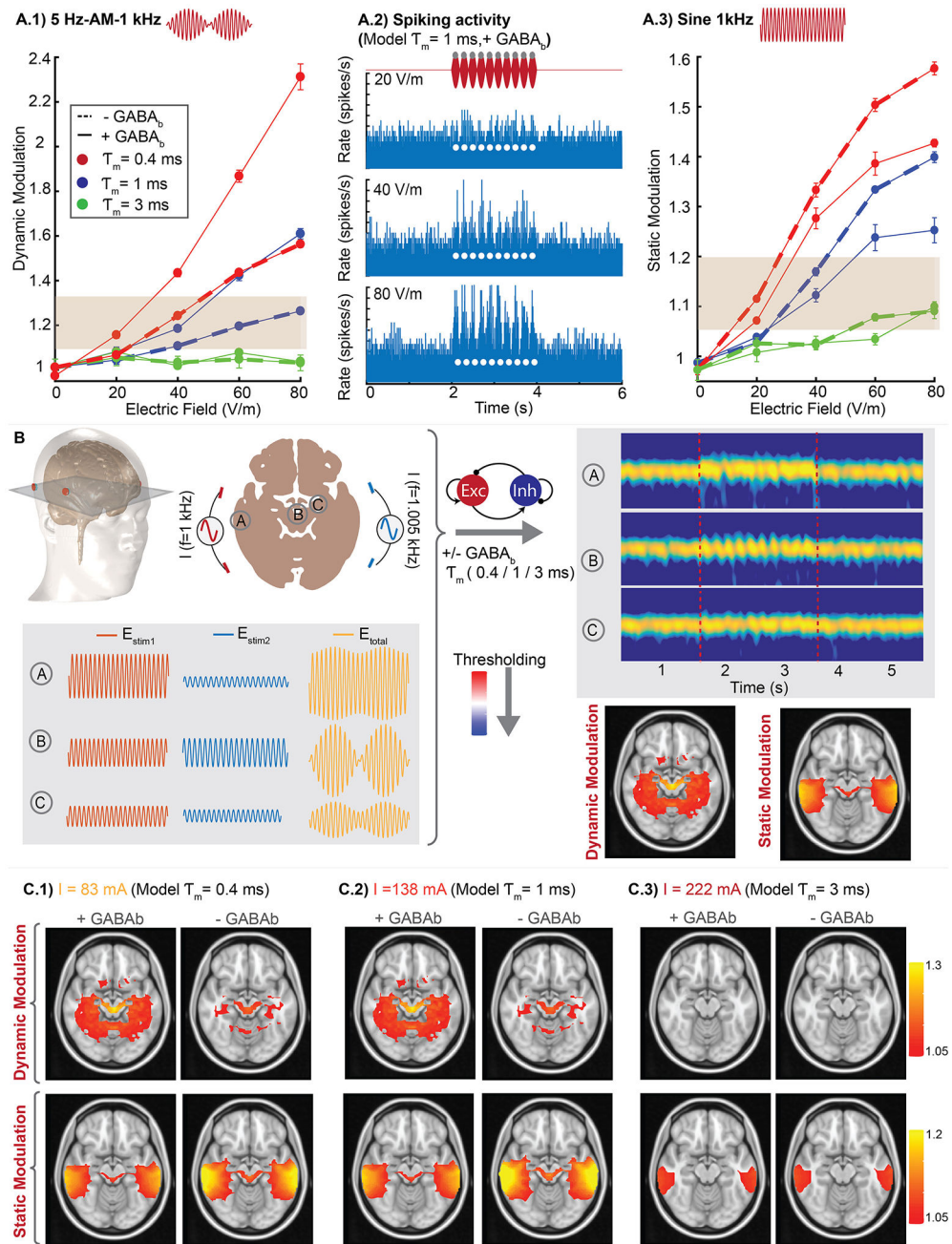
Fig. 3.
Generalized network model of temporal interference stimulation of oscillation. (A.1) Effect of membrane time constant (τ_m) and GABAergic inhibition on gamma modulation using amplitude-modulation (AM) waveform (5 Hz envelop and 1 kHz carrier frequency) with different field intensities. Each point represents mean (±SEM) of normalized gamma power for repeated runs of model (Blue solid line matches the experimental data of hippocampal gamma). A.2) Spiking activity for 5 Hz-AM-1 kHz stimulation using different electric field intensities. Y axis is clipped for illustration purposes in 80 V/m. A.3) Effect of membrane time constant and GABA$_b$ on gamma modulation using unmodulated 1 kHz sine waveform

with different electric field intensities. (**B**) Workflow for multi-scale model of dynamic and static modulation of oscillations across brain. Electric field for each voxel of brain was calculated using computational head model and used as I_{stim} in network model to generate corresponding modulation (both static and dynamic). (**C**) Model predictions for dynamic and static modulation using different network model parameters: $\tau_m = 0.4$ m s with/without $GABA_b$ inhibition (C.1), $\tau_m = 1$ m s with/whiteout $GABA_b$ inhibition (C.2), $\tau_m = 3$ m s with/without $GABA_b$ inhibition (C.3). Grey box in A.1 and A.3 indicates thresholds derived from experimental hippocampal recordings used in plotting static and dynamic modulation in panel C. White circles in A.2 indicates peaks of amplitude-modulated waveform.